UNIVERSITY OF WEST BOHEMIA

Applied and Computational Mechanics 2 (2008) 335–346

Applied and Computational Mechanics

Nonlinear vibrations and stability of aerostatic bearing

L. Půst[a,*], J. Kozánek[a]

[a] *Institute of Thermomechanics, Czech Academy of Sciences, Dolejškova 5, Prague, Czech Republic*

Received 10 September 2008; received in revised form 18 November 2008

Abstract

Bearings based on aerostatic principle belong to the new machine elements advantageous for low- and high-speed applications, but their dynamic and stability properties are not yet sufficiently known. This paper presents a new elaborated method and gained results of theoretical investigation of dynamic properties of aerostatic bearing in general dimensionless form. It is aimed also as a supporting tool for diagnostic and identification methods used at developing of new bearings proposed by TECHLAB, Prague for industrial applications. Mathematical model expresses nonlinear and evolutive properties in the entire area of bearing clearance, contains sufficient number of free parameters in functions of restoring and damping forces and can therefore describe all types of motions occurring in gas bearings as periodic, quasi-periodic, including beats and instability, which can leads to chaotic and self-excited vibrations. The influence of non-diagonal elements of stiffness and damping matrices of linearized model on the spectral properties and the stability of system is investigated, too.

Keywords: aerostatic bearing, nonlinear characteristic, linearized system, stability

1. Introduction

Aerostatic bearings are new machine elements applied both for high- and low-speed operation of rotors. Majority of researchers in the field of fluid — bearings focused their investigation on the oil journal bearings, but some interesting works oriented on gas bearings appeared in the last decades. Lot of them elaborate solution of gas flow in bearing clearance by means of Reynolds equations, few of them are devoted to the rotor dynamics and gas bearing properties. Let us mention A. Tondl [7] who presented solution of vertical rotor vibrations using linearized expression for stiffness and damping forces. Experimental procedure for ascertaining linear stiffness and damping parameters is described in [5]. Vertical test stand described in [6] is being used to validate gas bearing design model and show how to calculate stiffness and damping of bearing by means of synchronous excitation. Authors of [8] show the influence of nonlinear gas film forces on the stabilities of system's equilibrium position and unbalance responses, by experimental solution and by simple numerical model of characteristics based on assumption of exponential stiffness properties. A new type of slot-restricted gas journal bearings is studied in [9]. Short description of aerostatic thrust bearing is given in [10].

In order to gain reliable experimentally verified data for design of aerostatic bearings developed in our country by Techlab s.r.o., a project of GAČR No 101/06/1787, "Dynamic properties of gas bearings and their interaction with rotor" has been opened and elaborated. The experimental investigation of this project is based on using special adapted Rotor Kit Bently Nevada

*Corresponding author. Tel.: 420 266 053 212, e-mail: pust@it.cas.cz.

(RKBN) complemented by suitable measurement and loading apparatus for identification of static and dynamic characteristic of aerostatic journal bearings [1, 2].

The presented paper is a theoretical contribution to the analysis of dynamic properties of RKBN test stand with the aim to determine the effect of nonlinear characteristics and spectral dependences of diagonal and non-diagonal elements of stiffness and damping matrices. Obtained results will help by the quantitative and qualitative diagnostic analysis of aerostatic bearings behavior.

For these purposes a new description of nonlinear stiffness and damping properties valid in the entire clearance of bearing by means of mathematical expression with several free parameters is developed. A new treatment based on non-synchronous excitation with frequency different from rotor revolution is advantageous for more exact identification.

2. Scheme of test stand

The detailed description of RKBN structure including special arrangement of aerostatic bearing with apparatus measuring displacements in vertical and horizontal directions of test head aerostatic bearing, as well as excitations forces in both directions is given in [1, 2].

As distinct from the usual arrangement of rotor systems, the test head with bearing bush in the RKBN test stand is movable and supported only on a system of thin strings securing its purely transitional motion. Rigid test shaft is supported in two precise stiff rolling bearings. It rotates with angular velocity ω and its rotation axis is fixed in space without any motion. The simplified scheme for derivation of motion equations is shown in Fig. 1. Rigid rotor supported in two rolling bearings has axis of rotation z and its structure is symmetrical to the plane xy. It is driven by an electric motor controlled to speeds up to 10 000 rpm, i.e. up to $\omega = 1\,000\,\mathrm{s}^{-1}$. Test head contains aerostatic bearings surrounding the rotor of diameter $D = 30\,\mathrm{mm}$ with diameter clearance $2c = 0.08\,\mathrm{mm}$ and has mass 1.2 kg. Length of the bearing shell is $L = 1.5\,\mathrm{D} = 45\,\mathrm{mm}$, its pressurized air hose is connected with the bearing clearance by 16 orifices in two rows uniformly arranged along the circumference. Inlet air pressure was 0.2 or 0.4 MPa.

3. Forces in aerostatic bearing

Due to the axially symmetrical arrangement of test stand and axially symmetrical flow inlet of compressed air the force-displacement relation described in polar coordinates r, φ is inde-

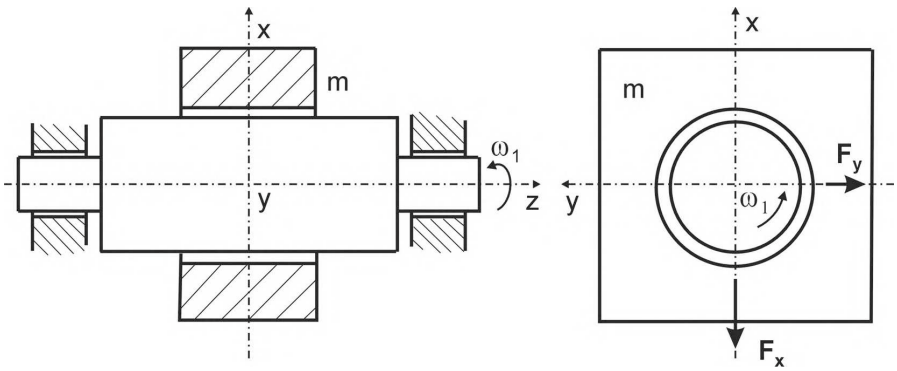

Fig. 1. Scheme of experimental stand

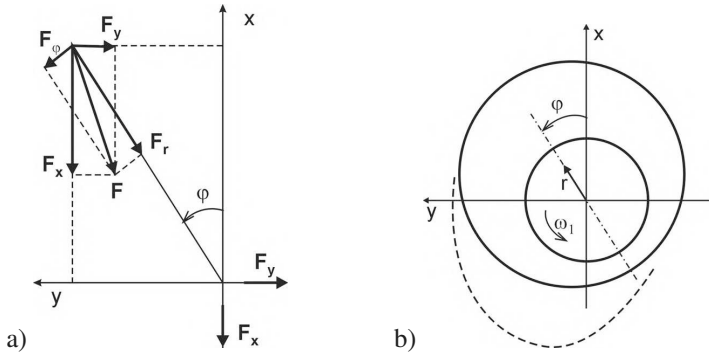

Fig. 2. a) Forces on test head, b) Displacement of test head

pendent on the angle φ (e.g. [7]). Therefore the reaction forces acting on test head at relative deviation r of test head centre against the rotor centre should be the same in all angular position φ. When the shaft does not rotate, the restoring reaction force is opposite to vector r. Situation at shaft rotation ω_1 is shown in Fig. 2a, where the reaction force has radial component $F_r(r)$ and tangential component $F_\varphi(r)$. Directions of these forces are influenced by unsymmetrical distribution of aerodynamic pressure (dashed line in Fig. 2b) in the clearance.

Transformation of these forces into components expressed in rectangular coordinates x, y gives

$$F_x = F_r \cos\varphi + F_\varphi \sin\varphi \qquad F_y = F_r \sin\varphi - F_\varphi \cos\varphi, \tag{1}$$

where the trigonometric functions of angle φ can be replaced by function of rectangular coordinates x, y:

$$F_x = F_r \frac{x}{\sqrt{x^2+y^2}} + F_\varphi \frac{y}{\sqrt{x^2+y^2}} \qquad F_y = F_r \frac{y}{\sqrt{x^2+y^2}} - F_\varphi \frac{x}{\sqrt{x^2+y^2}}. \tag{2}$$

Forces F_r, F_φ can be expressed by very complicated formula as seen from some results published e.g. in [10]. In order to construct sufficiently general description of aerostatic bearings properties, we must use functions containing great number of free parameters, which enable to fit a set of experimental data in a high approximation. In this paper we restrict our presentation only on low power of displacements and velocities, but the methodology can be used for more complex form as well. If we suppose that the reaction force F together with its components F_r, F_φ increase linearly with distance $r = \sqrt{x^2+y^2}$, than we can introduce stiffness k_r, k_φ:

$$F_r = k_r r, \qquad F_\varphi = k_\varphi r \tag{3}$$

and the equations (2) are

$$F_x = k_r x + k_\varphi y \qquad F_y = -k_\varphi x + k_r y \text{ or } \mathbf{F}_{real} = \begin{bmatrix} k_r & k_\varphi \\ -k_\varphi & k_r \end{bmatrix} \begin{bmatrix} x \\ y \end{bmatrix} = \mathbf{K}\mathbf{q}. \tag{4}$$

Tangential force F_φ, as well as cross-stiffness k_φ, has non-zero magnitude only at rotation: $\omega_1 > 0$. Let us supposed that it depends linearly on the second power of the shaft rotation velocity ω_1: $k_\varphi(\omega_1) = \omega_1^2 k_f$.

If the shaft does not rotate, the stiffness matrix $\mathbf{K}$ is diagonal

$$\mathbf{K}_{\omega=0} = \begin{bmatrix} k_r & 0 \\ 0 & k_r \end{bmatrix}. \tag{5}$$

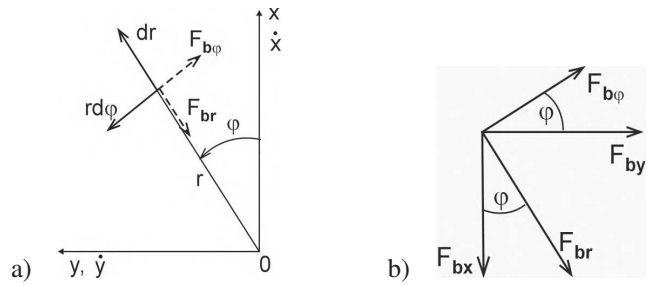

Fig. 3. a) Damping forces, b) Damping forces in rectangular coordinates

The same formal relations as (1, 2) are valid also for damping forces $F_{br}, F_{b\varphi}$, when the polar coordinates r, φ vary with the time t: $\dot{r} = \mathrm{d}r/\mathrm{d}t$, $r\dot{\varphi} = r\,\mathrm{d}\varphi/\mathrm{d}t$. Vector diagrams of velocities and corresponding reactions forces on test head are in Fig. 3, both in polar and rectangular coordinates. Their magnitudes are connected by relationships:

$$\begin{aligned} F_{bx} &= F_{br}\cos(\varphi) - F_{b\varphi}\sin(\varphi) = F_{br}\frac{x}{r} - F_{b\varphi}\frac{y}{r} \\ F_{by} &= F_{br}\sin(\varphi) + F_{b\varphi}\cos(\varphi) = F_{br}\frac{y}{r} + F_{b\varphi}\frac{x}{r}. \end{aligned} \tag{6}$$

For linear damping in the whole interval of coordinates $r \in (0, d)$, $\varphi \in (0, 2\pi)$, the damping forces vary proportionally to the velocities $\dot{r}$ and $r\dot{\varphi}$

$$F_{br} = b_r\dot{r}, \qquad F_{b\varphi} = b_\varphi r\dot{\varphi} \tag{7}$$

and the force components in rectangular coordinates are

$$F_{bx} = b_r\dot{r}\frac{x}{r} - b_\varphi\dot{\varphi}r\frac{y}{r} \qquad F_{by} = b_\varphi\dot{\varphi}r\frac{x}{r} + b_r\dot{r}\frac{y}{r}. \tag{8}$$

After expressing derivates $\dot{r}$ and $r\dot{\varphi}$ from transformation formula $x = r\cos\varphi$, $y = r\sin\varphi$

$$\dot{r} = \dot{x}\cos\varphi + \dot{y}\sin\varphi = \dot{x}\frac{x}{r} + \dot{y}\frac{y}{r} \qquad r\dot{\varphi} = -\dot{x}\sin\varphi + \dot{y}\cos\varphi = -\dot{x}\frac{y}{r} + \dot{y}\frac{x}{r},$$

we get

$$\begin{aligned} F_{bx} &= (b_r x^2 + b_\varphi y^2)\frac{\dot{x}}{r^2} + (b_r - b_\varphi)xy\frac{\dot{y}}{r^2} \\ F_{by} &= (b_r - b_\varphi)xy\frac{\dot{x}}{r^2} + (b_r y^2 + b_\varphi x^2)\frac{\dot{y}}{r^2}. \end{aligned} \tag{9}$$

This equations are simplified fundamentally if the damping field is isotropic $b_r = b_\phi = b$:

$$F_{bx} = b\dot{x} \qquad F_{by} = b\dot{y} \quad \text{and} \quad \mathbf{F_b} = \mathbf{B}\dot{\mathbf{q}} = \begin{bmatrix} b & 0 \\ 0 & b \end{bmatrix} \begin{bmatrix} \dot{x} \\ \dot{y} \end{bmatrix}.$$

In the general case of nonlinear, anisotropic stiffness and damping fields the general equations (2) and (6) have to be used. Equations (3) and (7) have to be replaced by

$$F_r(r, \omega_1, p), \quad F_\phi(r, \omega_1, p), \quad F_{br}(r, \omega_1, p), \quad F_{b\phi}(r, \omega_1, p), \tag{10}$$

where the nonlinear relationships on radial displacement r, angular velocity ω_1 and pressure of inlet air p are expressed.

4. Nonlinear and evolutive characteristics

4.1. Restoring (stiffness) characteristics

Because the components of restoring (elastic) forces in rectangular coordinate x, y are according to the equations (1) ascertained by means of the polar force components F_r and F_ϕ, the first step is oriented on the formulation of nonlinear function in these polar components. The simplest form is linear description given in (3) or without rotation in (5). Assumption of similar linear properties are used in many publications on aerostatic bearings, e.g. [1, 2, 3, 4, 5, 6], but there investigated motions of systems are solved very often as special cases around the shifted equilibrium positions, where the symmetry or asymmetry of matrices $\mathbf{K}, \mathbf{B}$ (eqs. 4, 8) cannot be used.

The breaking of symmetry is caused by the nonlinear properties of force-deflection characteristics of lubricated gas film. Let us suppose the nonlinear properties of restoring forces in the form of quadratic function of displacement r and of angular velocity ω_1:

$$F_r = (k_r + k_{r1} r^2 \omega_1^2) r, \qquad F_\varphi = (k_f \omega_1^2 + k_{\varphi 1} r^2 \omega_1^2) r, \tag{11}$$

where basic stiffness for our aim is $k_r = 1.41 \cdot 10^6\,\mathrm{Nm}^{-1}$ (see [3]) and coefficients k_f, k_{r1}, $k_{\phi 1}$ must be identified from experiments or from the solution of Reynolds equation [1, 2, 4]. In this numerical study, we focus on the investigation of influence of these coefficients on response of test head excited by external forces. In rectangular coordinate system x, y, there are components of elastic force after applying (2), (11):

$$\begin{aligned} F_{ex} &= (k_r + k_{r1}(x^2 + y^2)\omega_1^2)x + (k_f \omega_1^2 + k_{\varphi 1}(x^2 + y^2)\omega_1^2) y \\ F_{ey} &= -(k_f \omega_1^2 + k_{\varphi 1}(x^2 + y^2)\omega_1^2)x + (k_r + k_{r1}(x^2 + y^2)\omega_1^2) y. \end{aligned} \tag{12}$$

4.2. Damping characteristics

The nonlinear damping properties of aerostatic bearing can be supposed in the similar form as at stiffness i.e. in the form of damping coefficient proportional to quadratic function of displacement r and of angular velocity ω_1, which in polar coordinates gives

$$F_{br} = (b_r + b_{r1} r^2 \omega_1^2)\dot{r}, \qquad F_{b\varphi} = (b_\varphi + b_{\varphi 1} r^2 \omega_1^2) r\dot{\varphi}. \tag{13}$$

According to (1) we get for the damping force component in rectangular x, y coordinates

$$\begin{aligned} F_{bx} &= (b_r + b_{r1} r^2 \omega_1^2)\dot{r}\cos\varphi - (b_\varphi + b_{\varphi 1} r^2 \omega_1^2) r\dot{\varphi}\sin\varphi \\ F_{by} &= (b_r + b_{r1} r^2 \omega_1^2)\dot{r}\sin\varphi + (b_\varphi + b_{\varphi 1} r^2 \omega_1^2) r\dot{\varphi}\cos\varphi \end{aligned} \tag{14}$$

and using (8a)

$$\begin{aligned} F_{bx} &= (b_r + b_{r1} r^2 \omega_1^2)\frac{\dot{x}x^2 + \dot{y}xy}{r^2} - (b_\varphi + b_{\varphi 1} r^2 \omega_1^2)\frac{-\dot{x}y^2 + \dot{y}xy}{r^2} \\ F_{by} &= (b_r + b_{r1} r^2 \omega_1^2)\frac{\dot{x}xy + \dot{y}y^2}{r^2} + (b_\varphi + b_{\varphi 1} r^2 \omega_1^2)\frac{-\dot{x}xy + \dot{y}x^2}{r^2}. \end{aligned} \tag{14a}$$

Nonlinear damping characteristics can be expressed also in following form:

$$\begin{aligned} F_{bx} &= (b_r x^2 + b_\varphi y^2)\frac{\dot{x}}{r^2} + \omega_1^2(b_{r1}x^2 + b_{\varphi 1}y^2)\dot{x} + (b_r - b_\varphi)\frac{xy}{r^2}\dot{y} + (b_{r1} - b_{\varphi 1})\omega_1^2 xy\dot{y} \\ F_{by} &= (b_r - b_\varphi)\frac{xy}{r^2}\dot{x} + (b_{r1} - b_{\varphi 1})\omega_1^2 xy\dot{x} + (b_r y^2 + b_\varphi x^2)\frac{\dot{y}}{r^2} + (b_{r1}y^2 + b_{\varphi 1}x^2)\omega_1^2\dot{y}, \end{aligned} \tag{15}$$

where for numerical stability at $x = y = 0$: $r^2 = x^2 + y^2 + \varepsilon$, $\varepsilon = 1 \cdot 10^{-20}$.

5. Equations of test head motion

Equations of forced motion with frequency ω_1 and amplitude F_0 of movable test head at rotated shaft with velocity ω_1 and fixed axes are

$$\begin{aligned} m\ddot{x} + F_x + F_{bx} &= F_0 \cos\omega t + mg + F_{st} \\ m\ddot{y} + F_y + F_{by} &= F_0 \sin\omega t, \end{aligned} \tag{16}$$

where forces components F_x, F_{bx}, F_y, F_{by} are given in (12) and (14). So we get

$$m\ddot{x} + (k_r + k_{r1}(x^2+y^2)\omega_1^2)x + (k_f + k_{\varphi 1}(x^2+y^2))\omega_1^2 y + (b_r x^2 + b_\varphi y^2)\dot{x}/(x^2+y^2+\varepsilon) +$$

$$\omega_1^2(b_{r1}x^2 + b_{\varphi 1}y^2)\dot{x} + (b_r - b_\varphi)\frac{xy\dot{y}}{x^2+y^2+\varepsilon} + (b_{r1} - b_{\varphi 1})\omega_1 xy\dot{y} = F_0\cos(\omega t) + mg + F_{st}$$

$$m\ddot{y} + (k_r + k_{r1}(x^2+y^2)\omega_1^2)y - (k_f + k_{\varphi 1}(x^2+y^2))\omega_1^2 x + (b_r - b_\varphi)\frac{xy\dot{x}}{x^2+y^2-\varepsilon} +$$

$$\omega_1^2(b_{r1} - b_{\varphi 1})xy\dot{x} + (b_r y^2 + b_\varphi x^2)\frac{\dot{y}}{x^2+y^2+\varepsilon} + (b_{r1}y^2 + b_{\varphi 1}x^2)\omega_1^2\dot{y} = F_0\sin(\omega t).$$

In order to build general mathematical model for various type of aerostatic bearings with very different parameters, the transformation of the aforementioned equations into dimensionless form is recommended.

Dimensionless form of motion equations is advantageous also for numerical solution, as it always contains lower number of system parameters in comparison to the differential motion equations written in physical quantities. The fundamental physical parameters for this transformation are mass $m = 1.2\,\text{kg}$, radial gap $c = 0.04\,\text{mm}$, stiffness $k_r = 1\,410\,000\,\text{Nm}^{-1}$. Introducing 14 dimensionless quantities instead of 17 dimension ones:

$$\begin{aligned} \tau &= t\sqrt{\frac{k_r}{m}}, \quad X = \frac{x}{c}, \quad Y = \frac{y}{c}, \quad \eta = \omega\sqrt{\frac{m}{k_r}}, \quad \eta_1 = \omega_1\sqrt{\frac{m}{k_r}}, \quad \kappa_f = \frac{k_f}{m}, \\ \kappa_r &= k_{r1}\frac{c^2}{m}, \quad \kappa_\varphi = k_{\varphi 1}\frac{c^2}{m}, \quad f_0 = \frac{F_0}{k_r c}, \quad f_{st} = \frac{mg + F_{st}}{k_r c}, \\ \beta_r &= \frac{b_r}{\sqrt{k_r m}}, \quad \beta_\varphi = \frac{b_r}{\sqrt{k_\varphi m}}, \quad \beta_{r1} = b_{r1}\sqrt{\frac{k_r}{m}}\frac{c^2}{m}, \quad \beta_{\varphi 1} = b_{\varphi 1}\sqrt{\frac{k_r}{m}}\frac{c^2}{m} \end{aligned} \tag{17}$$

we get dimensionless form of motion equations (16)

$$\begin{aligned} &X'' + X + \eta_1^2(\kappa_f Y + (X^2+Y^2)(\kappa_r X + \kappa_\varphi Y)) + \frac{(\beta_r X^2 + \beta_\varphi Y^2)X'}{X^2+Y^2+\varepsilon} + \\ &\eta_1^2(\beta_{r1}X^2 + \beta_{\varphi 1}Y^2)X' + \frac{(\beta_r - \beta_\varphi)XYY'}{X^2+Y^2+\varepsilon} + (\beta_{r1} - \beta_{\varphi 1})\eta_1^2 XYY' = \\ &= f\cos(\eta\tau) + f_{st} \\ &Y'' + Y + \eta_1^2(-\kappa_f X + (X^2+Y^2)(\kappa_r Y - \kappa_\varphi X)) + \frac{(\beta_r - \beta_\varphi)XYX'}{X^2+Y^2+\varepsilon} + \\ &(\beta_{r1} - \beta_{\varphi 1})\eta_1^2 XYX' + \frac{(\beta_r Y^2 + \beta_\varphi X^2)Y'}{X^2+Y^2+\varepsilon} + \eta_1^2(\beta_{r1}Y^2 + \beta_{\varphi 1}X^2)Y' = f_0\sin(\eta\tau). \end{aligned} \tag{18}$$

These equations are numerically solved in following chapter.

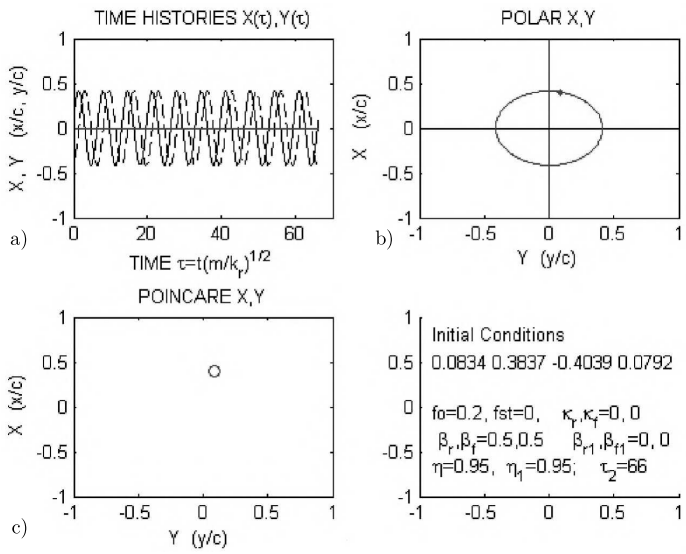

Fig. 4. Periodic stable oscillations

6. Examples

Let us show some selected cases of application of derived mathematical model for solution of head test motion. From 14 dimensionless parameters describing this model 6 of them let have in Fig. 4–7 fix values: $f_0 = 0.2$, $\eta = \eta_1 = 0.95$, $\beta_r = \beta_\phi = 0.5$, $\kappa_\varphi = 0$, three of them are variables (X, Y, τ) and the remaining 5 can be selected.

Response of vibrating system for values

$$f_{st} = 0, \quad \kappa_r = \kappa_f = 0, \quad \beta_{r1} = \beta_{\phi 1} = 0$$

is shown in Fig. 4. The motion is periodic with constant amplitudes as seen both from time histories $X(\tau), Y(\tau)$ in subplot a) and polar trajectories X, Y (subplot b). The Poincaré map in subplot c) concentrates into one point, representing the stable periodic state of system recorded at $\eta\tau = (2n + 1/2)\pi$, $n = 0, 1, 2, \ldots$

Cubic nonlinearities in characteristics of restoring forces given by nonzero parameters $\kappa_r = \kappa_\phi = 2$ at ($f_{st} = 0$, $\beta_{r1} = \beta_{\phi 1} = 0$) changes the response into quasi-periodic beats (Fig. 5a, b), again stable as seen from the Poincaré mapping on Fig. 5c where the representing points form a cluster similar to a closed circle.

Adding nonlinear damping forces given by positive parameters $\beta_{r1} = \beta_{\phi 1} > 0$ does not influence the system stability, it changes moderately only amplitudes of oscillations. However the effect of non-symmetry in β_{r1} and $\beta_{\phi 1}$ is very strong.

An example of response of system by nonlinear damping with different parameters $\beta_{r1} = 0.2$ and $\beta_{\phi 1} = -0.025$ is recorded in Fig. 6, where the very small disturbances slowly increase during the time and at $\tau > 90$ begin to be very decisive, which become evident by a sudden exponential rise of amplitudes. This loss of stability is clearly seen both at time histories $X(\tau)$, $Y(\tau)$ in Fig. 6a, and in polar trajectory X, Y in Fig. 6b. Due to the limited number of recorded periods of excitation, this instability is in Fig. 6c presented only by 2 points.

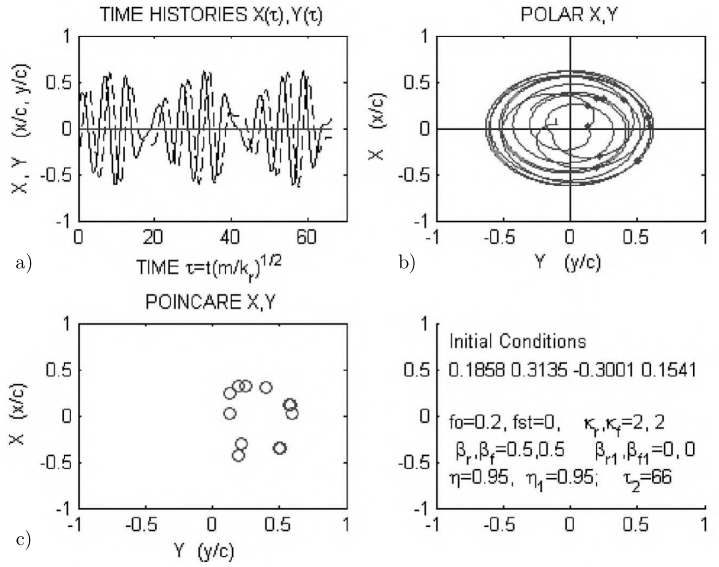

Fig. 5. Quasi-periodic oscillations (beats)

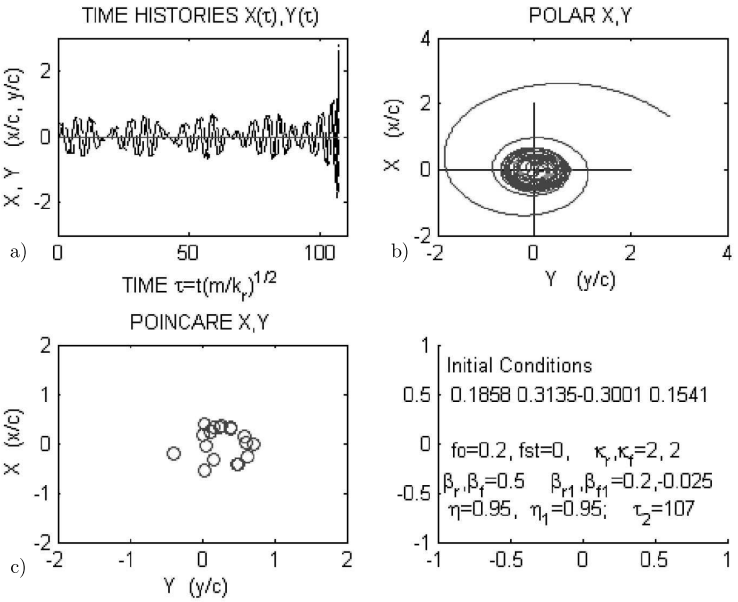

Fig. 6. Quasi-periodic oscillations, lost of stability

Another type of instability is shown in Fig. 7, where free vibrations ($f_0 = 0$) at small initial condition increase exponentially from the beginning at $\tau = 0$ to the unlimited values. This phenomenon is caused by the difference between linear damping coefficients $\beta_r = 0.1$ and $\beta_\phi = -0.1$.

Static load (weight mg and/or external force) causes vertical shift of X trajectory, both in time history $X(\tau)$ and in polar diagram X, Y, as it is shown in Fig. 8 for dimensionless load $f_{st} = (mg + F_{st})/(k_r c) = 0.7$ and for excitation amplitude $f_0 = 0.1$.

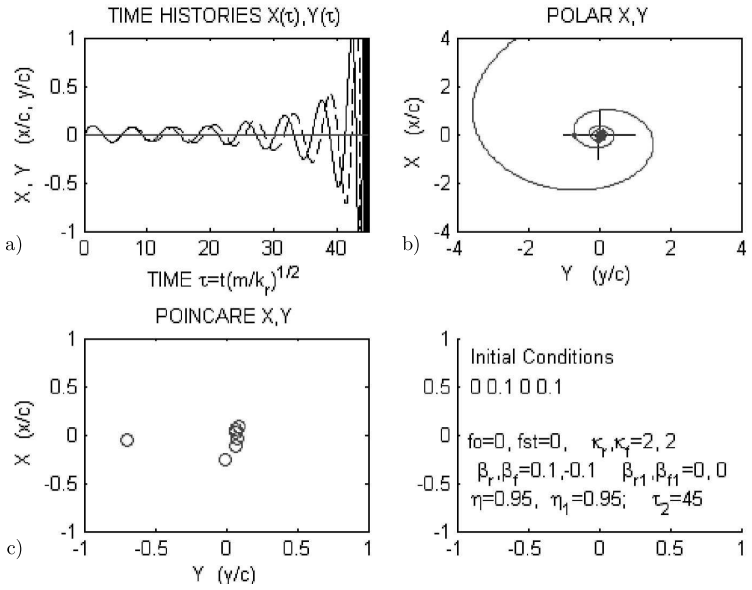

Fig. 7. Instability at small disturbances

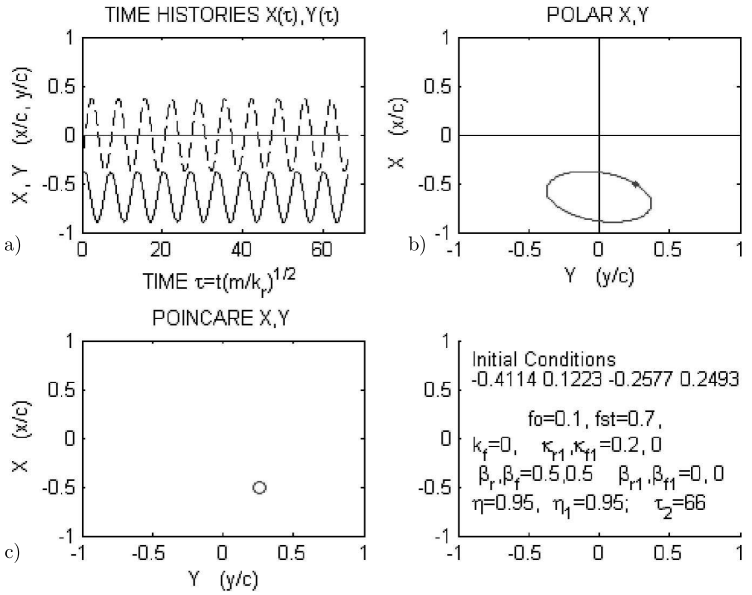

Fig. 8. Shift from static load $f_{st} = 0.7$

7. Model of linearized system

The test head was during preliminary measurements loaded by vertical gravitational force mg and excited by a small harmonic force. The mathematical model can be in that case simplified to the linear part of restoring and damping forces. Equilibrium position is on vertical axis

($|y| \to 0$) and linearized model according to the simplified equation (16) can be written for fixed rotation of rotor as

$$\mathbf{K}\mathbf{q}(t) + \mathbf{B}\dot{\mathbf{q}}(t) + \mathbf{M}\ddot{\mathbf{q}}(t) = \mathbf{F}(t), \tag{19}$$

where

$$\mathbf{q}(t) = \begin{bmatrix} x(t) \\ y(t) \end{bmatrix}, \quad \mathbf{F}(t) = F_0 \begin{bmatrix} \cos\omega t \\ \sin\omega t \end{bmatrix}, \quad \mathbf{K} = \begin{bmatrix} k_r & k_\varphi \\ -k_\varphi & k_r \end{bmatrix},$$

$$\mathbf{B} = \begin{bmatrix} b_r & b_\varphi \\ -b_\varphi & b_r \end{bmatrix}, \quad \mathbf{M} = \begin{bmatrix} m & \\ & m \end{bmatrix}.$$

The mathematical model is aimed for the spectral and modal analysis with the emphasize to determination of the level of stability motion of system expressed by real parts of complex eigenvalues. Corresponding homogeneous equation in complex amplitude form ($\mathbf{q}(t) = \mathbf{q}, e^{st}$, $\mathbf{q} \in C^2$) is

$$(\mathbf{K} + s\mathbf{B} + s^2\mathbf{M})\mathbf{q} = \mathbf{o} \tag{20}$$

and complex eigenvalues and eigenvectors are calculated by means of the so-called state space method. Numerical values of dynamic parameters for this analysis are given by measurements, by theoretical study — [4] and corrected by the identification — [1, 2] of the experimental stand — [3].

While the diagonal elements of matrices $\mathbf{K}, \mathbf{B}$ are determined from theoretical mathematical models and experimentally with a good accordance, the uncertainty of non-diagonal elements is greater. For this reason we shall analyze the influence of this (non-symmetric) parameters to the spectral and stability properties. For purposes of our project, during the numerical simulation we will in this paper apply following fixed values:

$$m = 1.2\,\text{kg}; \quad k_r = 1.41 \cdot 10^6\,\text{N/m}; \quad b_r = 500\,\text{Ns/m},$$

the influence of non-diagonal elements will be investigated in the ranges $k_\varphi \in \langle 10^2, 6 \cdot 10^5 \rangle$, $b_\varphi \in \langle 10, 4 \cdot 10^2 \rangle$. On the Fig. 9 are Real (s_j), Imag (s_j), $j = 1, 2$ as a function of parameter $p_B = b_\varphi$ for fixed $k_\varphi = 10^5\,\text{N/m}$. The parametric graph of s_j, $j = 1, 2$ in complex plane as a function of parameter $p_B = b_\varphi$ for fixed $k_\varphi = 10^5\,\text{N/m}$ is on the Fig. 10. Similarly, on the Fig. 11, 12 are depicted spectral values as a function of parameter $p_K = k_\varphi$ for fixed $b_\varphi = 10^2\,\text{Ns/m}$.

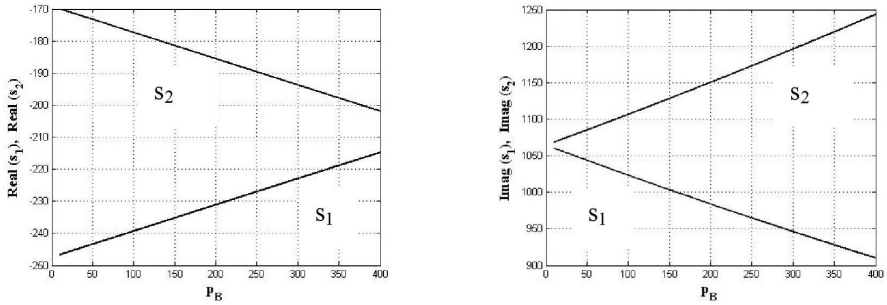

Fig. 9. Real (s_j), Imag (s_j), $j = 1, 2$ as a function of parameter p_B

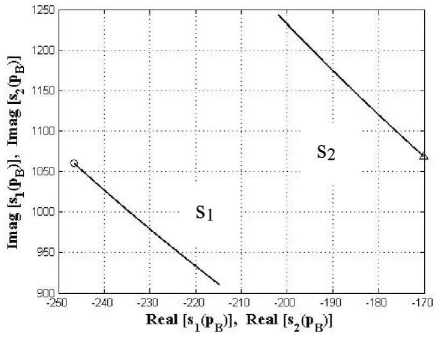

Fig. 10. Parametric graph of s_j, $j = 1, 2$ in complex plane as a function of parameter p_B. Initial points are marked by o, Δ

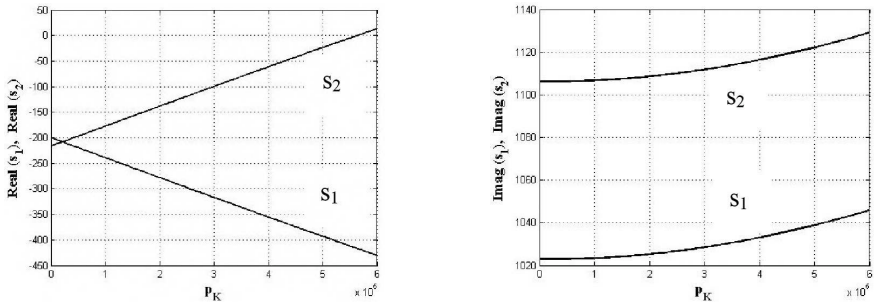

Fig. 11. Real (s_j), Imag (s_j), $j = 1, 2$ as a function of parameter p_K

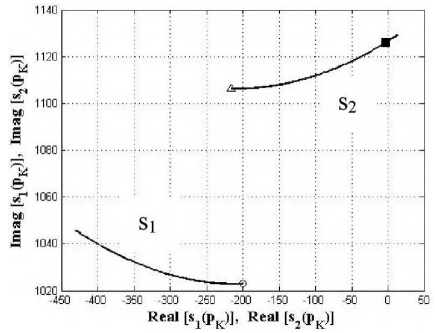

Fig. 12. Parametric graph of s_j, $j = 1, 2$ in complex plane as a function of parameter p_K. Initial points are marked by o, Δ and limit of stability motion by ▪

8. Conclusion

Mathematical model containing sufficient number of free parameters in functions describing both restoring and damping forces in aerostatic bearings was derived as a tool for qualitative and/or quantitative analysis of dynamic properties of new bearings developed in project GACR No. 101/06/1787.

Presented method of solution can be generalized also for other types of bearings by using another functions (not only cubic) expressing aerostatic and aerodynamic forces in polar coordinates r, ϕ, or after transformation in rectangular coordinates x, y.

Derived expressions are valid in the entire area of bearing clearance, all types of motions can be investigated with only limitation $r < c$.

Examples in the paper illustrate possibility of modeling different types of test head motions: Periodic, quasi-periodic, beats, instability, as well as shift of trajectories due to the static loading.

The influence of non-diagonal elements of stiffness and damping matrices of linearized dynamical system on the complex eigenvalues was presented in the numerical examples. For given range of non-diagonal elements, the changes of eigenfrequencies and the influence of non-diagonal elements of damping matrix was relatively small.

On the other hand, the increasing non-symmetry of the stiffness matrix leads to the non-stability of motion caused by the change of sign of real part of the second eigenvalue.

Acknowledgements

This work was supported by the Grant Agency of CR, project No. 101/06/1787 “Dynamic properties of gas bearings and their interaction with rotor”.

References

[1] J. Šimek, J. Kozánek, P. Steinbauer, Dynamic properties of earostatic journal bearings, Colloquium Dynamics of Machines 2007, IT ASCR, Prague, 2007, p. 177–184.

[2] J. Šimek, J. Kozánek, P. Steinbauer, Z. Neusser, Determination of earostatic journal bearings dynamic properties, Colloquium Dynamics of Machines 2008, IT ASCR, Prague, 2008, p. 161–168.

[3] J. Šimek, J. Kozánek, P. Steinbauer, Z. Neusser, Using Rotor Kit Bently Nevada for experiments with aerostatics bearings, TMM08, TU, Liberec, 2008.

[4] A. Skarolek, J. Kozánek, Computation of dynamic properties of earostatic journal bearings, Engineering mechanics 2007, Svratka, 2007, CD-ROM edition, p. 12.

[5] Ch. T. Hatch, R. G. Colwell, M. J. Murray, J. B. Gillis, D. E. Bently, Stiffness and damping results from perturbation testing of externally pressurized radial gas bearings, ISCORMA-4, Calgary, 2007, CD-ROM edition, paper 301, p. 11.

[6] Ch. T. Hatch, R. G. Colwell, M. J. Murray, D. E. Bently, A rotordynamic model for use in high-speed gas bearing testing, ISCORMA-4, Calgary, 2007, CD-ROM edition, paper 313, p. 12.

[7] A. Tondl, Vibration of rigid rotors with vertical shafts mounted in aerostatic bearings, Monographs and memoranda No. 14, SVUSS, Běchovice, 1973, 80 pages.

[8] V. Barzdaitis, V. Zemaitis, V. V. Barzdaitis, R. Didziokas, Stability of rotor with gas-lubricated journal bearing, The archive of mechanical engineering, LIV, 2007 No. 2, p. 167–175.

[9] J. K. Park, K. W. Kim, Stability analyses and experiments of spidle system using new type of slot-restricted gas journal bearings, Tribology International 37 (2004) p. 451–462.

[10] J. P. Khatait, W. Lin, W. J. Lin, Design and development of orifice type of aero static thrust bearing, SIMTech technical report, Vol. 6, 2005, No. 1, p. 7–12.